Dalton Transactions

Cite this: *Dalton Trans.*, 2011, **40**, 8206

www.rsc.org/dalton

PAPER

Substituted pyridazines as ligands in homoleptic (*fac* and *mer*) and heteroleptic Ru(II) complexes†

Gareth Cooke, Gearóid M. Ó Máille, Roberto Quesada, Longsheng Wang, Sunil Varughese and Sylvia M. Draper*

Received 28th February 2011, Accepted 25th May 2011
DOI: 10.1039/c1dt10340g

This article reports the preparation of a range of phenyl, pyridyl and pyrazinyl substituted pyridazines *via* the inverse electron demand [2 + 4] Diels–Alder reaction between 3,6-di(2-pyridyl)-1,2,4,5-tetrazines (bptz) and 3,6-di(2-pyrazinyl)-1,2,4,5-tetrazines (bpztz) and suitable dienophiles including acenaphthalene. The resulting polyaromatic compounds vary systematically in the number of aromatic substituents and the number and position of N-heteroatoms. For four of these compounds, the effect of the molecular changes on the solid-state structures were investigated using single crystal X-ray crystallography. The pyridazines were used as bidentate ligands in {M(II)(bipy)$_2$} and *tris*(homoleptic) complexes (M = Fe, Ru). The optical and electrochemical properties of these complexes reflect the electron accepting character of the new ligands. The facial and meridional isomers of the *tris* complexes could be separated by column chromatography (on silica), thus allowing a spectral comparison of their absorption and emission properties. The solid-state structures of several of the metal complexes are discussed, including that of the facial isomer of the *tris* Ru(II) complex of 3,6-bis(2-pyridyl)-4,5-bis(4-pyridyl)pyridazine—a potential preformed geometric motif for the predirected construction of supramolecular assemblies.

Introduction

This work forms part of a long-standing interest in N-containing polyphenylenes both as synthons in the formation of heteroatomic graphenes and as ligands in co-ordination chemistry.[1–3] In our synthetic development of N-containing polyaromatic compounds we have established protocols for the [2 + 4] cycloaddition of appropriately substituted alkynes and nitriles to cyclopentadienone derivatives. In order to introduce higher levels of N-doping in the resulting systems our attention has turned to substituted tetrazines as precursors to pyridazines. Such compounds were attractive because tetrazines, particularly 3,6-di(2-pyridyl)-1,2,4,5-tetrazine (bptz) have been used as dienes in inverse electron demand Diels–Alder reactions for many years. Indeed pyridazine-derived assemblies generated synthetically in this manner have been used previously by the authors to demonstrate the importance of C–H$\cdots\pi$, $\pi\cdots\pi$ and numerous weak C–H$\cdots$N interactions in the stabilisation of supramolecular architectures.[4]

Another favourable aspect of this chemistry is the retention of the rich co-ordination chemistry of the tetrazine[5] in the resulting pyridazine-derivatives, thus providing access to a variety of transition metal complexes[6] and a useful set of systematic building blocks for the construction of supramolecular systems.[7–9] 3,6-Di(2-pyridyl)pyridazine, for example, is a popular bidentate chelating ligand in coordination chemistry, and complexes a wide range of metals including iridium and palladium.[10,11] As highly adaptable ligands, pyridazines have also been used for the construction of supramolecular frameworks containing silver and copper.[12,13] Constable and co-workers have prepared pyridazyl-centred ligands by reacting bptz with a variety of substituted alkynyl dienophiles; reporting the supramolecular self-assembly of some of these pyridazyl ligands with silver salts.[14]

The work herein describes the synthesis of both homoleptic ruthenium and iron and heteroleptic ruthenium *bis*(bipyridine) complexes of the form [Ru(L)(bpy)$_2$]$^{2+}$. Such systems possess valuable chemical and spectral properties, *e.g.* metal to ligand charge transfer (MLCT) in the visible region, and long lived excited states. The inertness of the Ru(II) centre also allows the study of redox behaviour without complications arising from ligand substitution or exchange.[15] The *tris*(homoleptic) complexes of the systems presented offer considerable possibilities as supramolecular building blocks due to the ease with which multiple secondary coordination sites can be built into the ligand. However, ideally in order to exploit this potential, the separation of the meridional and facial isomers should be demonstrated.

School of Chemistry, University of Dublin, Trinity College, Dublin 2, Ireland. E-mail: smdraper@tcd.ie; Fax: (+353)-1-671-2826

† Electronic supplementary information (ESI) available: full experimental details. CCDC reference numbers 812335–812342. For ESI and crystallographic data in CIF or other electronic format see DOI: 10.1039/c1dt10340g

The presence of only one isomer leads to a more predictable geometric platform on which to build supramolecular structures. In general, *fac* isomers of coordination complexes have proven most valuable in this regard due to their inherent C_3 symmetry, which gives greater directional control in the formation of assemblies such as helicates. Unfortunately the formation of *fac* isomers in *tris* complexes is statistically disfavoured, and *fac* selective syntheses have only been achieved *via* tethering the chelating groups, as demonstrated by Weizman *et al.*[16] and further developed by Fletcher.[17]

The separation of facial and meridional isomers is a challenging undertaking, and consequently few examples are found in the literature. Of the reported methods for such isomeric separation (including sublimation,[18] HPLC[19] and ion-exchange assisted Sephadex chromatography[20,21]), it was found that conventional preparative chromatography[18,22,23] was sufficient to effect the separation of the *mer* and *fac* isomers reported herein.

Results and discussion

The Diels–Alder reaction of bptz and bpztz (synthesised according to literature procedures[24,25]) and suitable dienophiles gave rise to novel pyridazine centred ligands (Scheme 1). In the reaction of 2-acetyl pyridine with bptz, the ketone functional group was activated using a 10% methanolic solution of KOH, allowing for an 80% yield of **1a**. Diels–Alder reactions involving acetylene-derived dienophiles required more extreme reaction conditions: 5-ethynylpyrimidine and bptz were refluxed for 24 h in toluene to give a 65% yield of **2a**. In both reactions the products were purified by column chromatography.

In the case of alkene-derived dienophiles, the resulting dihydropyridazinyl Diels–Alder adduct must be oxidized to furnish the aromatic pyridazine product. The reactions of bptz with *trans*-stilbene, 1,2-di(4′-pyridyl)ethene and 3,3′,5,5′-tetramethoxy stilbene led to yields of 92%, 75% and 61%, respectively. After purification by column chromatography these were oxidised using nitrous oxide gas to yield the pyridazine-derived ligands **3a**, **4a** and **5a** in yields of 74%, 50%, and 75%, respectively. **6** has been reported elsewhere[6] and **3a** has been synthesised previously from diphenylacetylene by Constable and co-workers.[14]

The same procedures were used to generate compounds **1b–4b**. The yields of these reactions were generally lower and their metal complexes deviate little from their bptz-derived counterparts.

Heteroleptic complexes $[Ru(1a–6)(bpy)_2][PF_6]_2$

The ruthenium(II) *bis*(bpy) complexes of **1a–6** were prepared by refluxing the ligands with $[Ru(bpy)_2Cl_2]$ in ethylene glycol and water for 4–6 h (Scheme 2). The complexes were isolated in good yield as their PF_6 salts and purified by column chromatography.

Ruthenium(II) and iron(II) *tris*(homoleptic) complexes

The ruthenium(II) *tris*(homoleptic) complexes of **3a**, **4a** and **5a** were prepared on reflux with $RuCl_3$ and *N*-ethyl morpholine in ethylene glycol for 72 h. Following precipitation with saturated KPF_6, the two geometric isomers were separated using preparative TLC plates. The particularly low yield of the complex $[Ru(\mathbf{5a})_3][PF_6]_2$ (*mer* 5%, *fac* 3%) arose as a result of the need to further purify the *mer* isomer *via* preparative TLC.

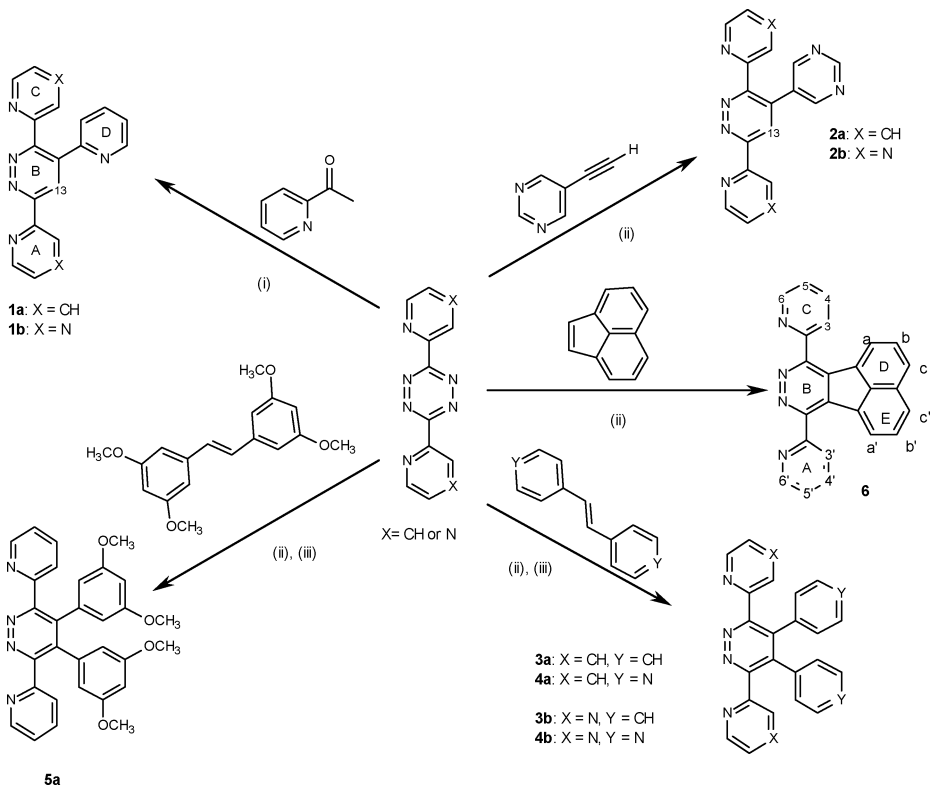

Scheme 1 Synthesis of pyridazine derivatives. (i) Stirred at R.T. in THF with KOH; (ii) toluene, reflux overnight; (iii) nitrous oxide gases, CH_2Cl_2.

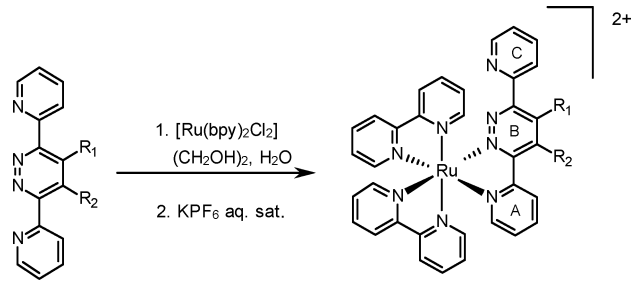

Scheme 2 The synthesis of [Ru(**1a–6**)(bpy)$_2$][PF$_6$]$_2$.

The iron(II) *tris* complexes were prepared from **3a**, **4a** and **5a** with an excess of Fe(BF$_4$)$_2$ in acetonitrile. The *mer* and *fac* isomers were again separated by column chromatography and/or TLC plates. (Reaction conditions summarised in Scheme 3.)

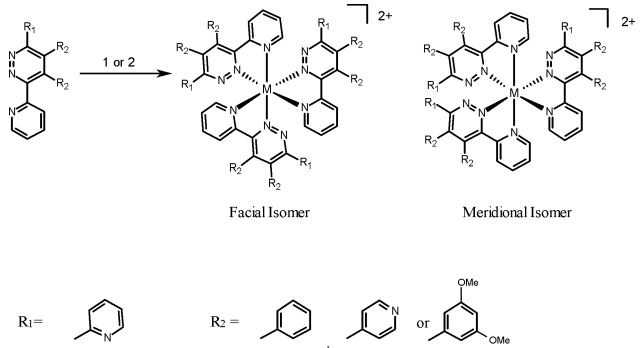

Scheme 3 Synthesis of [M(**3a–5a**)$_3$]$^{2+}$ (M = Fe, Ru). 1: RuCl$_3$, *N*-ethyl morpholine, ethylene glycol, 170 °C, 72 h; 2: Fe(BF$_4$)$_2$, acetonitrile, 60 °C, 2 h.

Characterization of [Ru(1a–6)(bpy)$_2$][PF$_6$]$_2$

In order to facilitate NMR characterisation of the ruthenium(II) *bis*(bipyridyl) complexes of **1a**, **2a**, **3a**, and **4a**, [Ru(**1a–4a**)(bpy)$_2$]$^{2+}$, the analogous deuterated bipyridine (bpy$_{d8}$) complexes were synthesised. As illustrated in Fig. 1 for [Ru(**2a**)(bpy)$_2$]$^{2+}$, the removal of the bipyridine signals vastly simplifies the ^{1}H NMR spectra. The two 2-pyridyl ring systems were differentiated on the basis of nOe experiments. These indicated a through-space interaction between the proton at C13 on the pyridazine ring in **1a** and **2a**, (see Scheme 1 for atom labelling) and the adjacent proton on the co-ordinated pyridyl ring. Full assignment was achieved using a range of 2-D TOCSY NMR experiments.

The ^{1}H NMR spectrum of [Ru(**6**)(bpy)$_2$]$^{2+}$ was well resolved, allowing satisfactory characterisation without resorting to the use of bpy$_{d8}$. Analysis of the ^{1}H–^{1}H COSY showed two three-spin systems (arising from the fluoranthene portion) and six four-spin systems (the pyridyl portions of bpys and **6**). ROESY experiments revealed a single interaction between a fluoranthene and a pyridyl spin system—indicating H3′ of the co-ordinated (fixed) pyridine of **6** (ring A) and its closest neighbouring proton, a′ on ring E (see Scheme 1). Further evidence supporting this assignment was obtained by inversion recovery experiments—five of the four-spin systems (excluding ring C) recovered from inversion within 0.8 s. The remainder took over 2.5 s and was assigned as the non-coordinated ring C, the only ring which could not recover

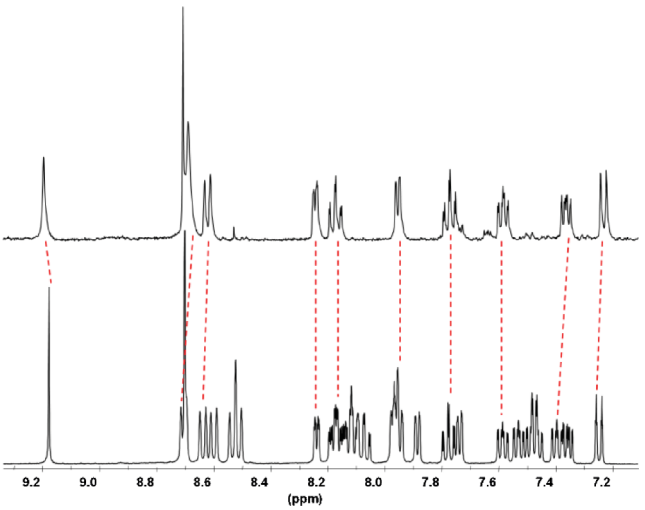

Fig. 1 The ^{1}H-NMR spectra of the non-deuterated bpy complex [Ru(**2a**)(bpy)$_2$][PF$_6$]$_2$ (bottom), compared with the deuterated bpy Ru(II) complex [Ru(**2a**)(bpy$_{d8}$)$_2$][PF$_6$]$_2$ (top) (CD$_3$CN, RT, 600 MHz). Full assignment can be found in the ESI.†

through the relaxation pathways provided to the other rings by the co-ordinated metal centre. Signals within each spin system were again assigned using selective TOCSY experiments. The ^{1}H NMR spectrum of [Ru(**5a**)(bpy)$_2$]$^{2+}$ was assigned similarly.

UV-Vis spectroscopy

The UV-Vis absorption spectra of the [Ru(**1a–5a**)(bpy)$_2$][PF$_6$]$_2$ complexes are shown in Fig. 2. They are quite similar to that of [Ru(bpy)$_3$]$^{2+}$, though the absorbance in the visible region is broader, consisting of two MLCT bands. The most red-shifted of these (≅ λ 485 nm) arises from the pyridazine derived ligand (dπ → π_1*). The other band (≅ λ 428 nm) is ascribed to an MLCT of the bpy ligands, or to a HOMO–SLUMO (second lowest unoccupied molecular orbital) transition (dπ→π_2*).[26] The absorption maximum at ≅ λ 280 nm is a ligand-centred transition and varies only slightly from one complex to another. The spectrum of [Ru(**6**)(bpy)$_2$][PF$_6$]$_2$ is different from the others: the introduction of the aromatic fluoranthene to the molecule causes some structured ligand-centred absorptions to be observed

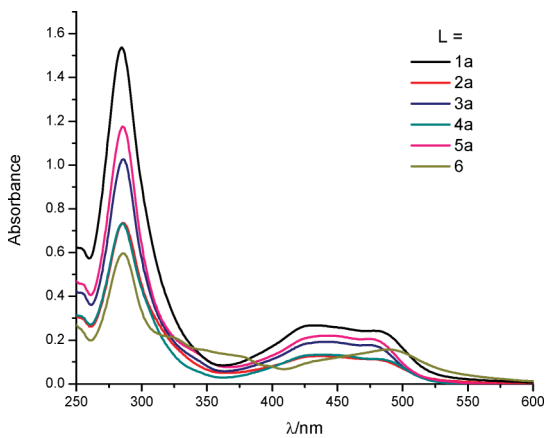

Fig. 2 The UV-Vis absorption spectra of the complexes [Ru(**1a–6**)(bpy)$_2$][PF$_6$]$_2$ (2×10^{-5} M in CH$_3$CN).

at ~ λ 350 nm and the highest energy ^{1}MLCT band is less intense. Enhanced aromaticity also lowers the energy of the ligand's π* orbitals, resulting in the most red shifted ^{1}MLCT-pyridazine absorption in the series.

The emission spectra of complexes [Ru(**1a–6**)(bpy)$_2$][PF$_6$]$_2$ are shown in Fig. 3, excitation into either of the two MLCT absorption maxima exhibited by these compounds, results in the same red emission. Complexes of ligands **3a** and **5a** emit at a slightly shorter wavelength (λ_{em} = 670 nm for both) than those of **1a**, **4a** and **6** (λ_{em} = 700 nm, 710 nm and 710 nm, respectively). The lower energy emission of the latter may be due to the electron-withdrawing character of nitrogen-rich substituents on **1a** and **4a**, and is a consequence of the aromaticity of the fluoranthene portion of **6**.

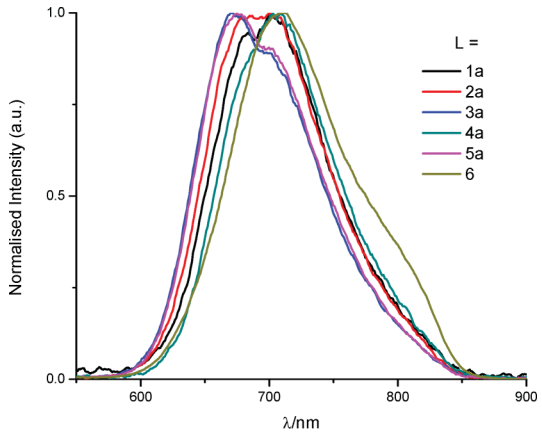

Fig. 3 Normalised emission spectra of the complexes [Ru(**1a–6**)(bpy)$_2$][PF$_6$]$_2$ (2×10^{-5} M in CH$_3$CN).

Electrochemistry

The redox potentials associated with [Ru(**1a–6**)(bpy)$_2$][PF$_6$]$_2$ are shown in Table 1. The first ligand reduction in each case was assigned to the pyridazine-centred ligand, as their lower energy π* orbitals (compared to bpy) ensure that these are more easily reduced.[27] The second and third highly consistent reductions are assigned to the bpy ligands, though there are pyrimidyl complexes known where the second reduction is thought to occur preferentially on the non-bpy ligand.[28] The values of the oxidation potentials indicate the effect of the pyridazine-centre on the electrochemistry of the complexes; its lower pK_a (an indicator of lower σ-bonding strength) relative to pyridine results in higher Ru(II/III) oxidation potentials. The final column in Table 1 provides the $\Delta E_{\frac{1}{2}}$ values of each of the six complexes, calculated by subtracting the first reduction potential of each complex from its oxidation potential. These values give an indication of the HOMO–LUMO energy gap and correlate with the position of the MLCT emissions. [Ru(**5a**)(bpy)$_2$][PF$_6$]$_2$ has the highest energy emission (λ_{max} 670 nm) and the largest $\Delta E_{\frac{1}{2}}$ (2.51 V). Similarly [Ru(**6**)(bpy)$_2$][PF$_6$]$_2$, having the lowest energy emission, λ_{max} 710 nm, has the smallest $\Delta E_{\frac{1}{2}}$ value (2.22 V). Although $\Delta E_{\frac{1}{2}}$ values can have error values of up to ± 20 mV, the results were found to be highly reproducible.

Ruthenium(II) *tris*(homoleptic) complexes of ligands 3a–5a

The ^{1}H NMR spectra of the *mer* isomers of the ruthenium(II) *tris* complexes of ligands **3a**, **4a** and **5a** consisted of many overlapping signals and only the most highly shielded and deshielded signals could be assigned (see ESI†). 2D-NMR experiments and the C_3 symmetry of the *fac* isomers aided spectral assignments. The ^{1}H-NMR spectrum of *fac*-[Ru(**3a**)$_3$][PF$_6$]$_2$ is shown colour coded in Fig. 4. The H3 protons are expected to be shielded by the neighbouring ring current; H3′ of ring A experiences this effect to the greatest extent as it has no freedom to rotate. On this basis the two 2-pyridyl rings were differentiated using 2-dimensional NMR TOCSY experiments. The two phenyl rings give rise to two separate sets of signals, TOCSY NMR experiments show that one ring exhibits three sharp peaks whereas the other displays two broad signals which sharpen and shift at higher temperatures. Full details of the NMR assignments of these complexes are given in the ESI.†

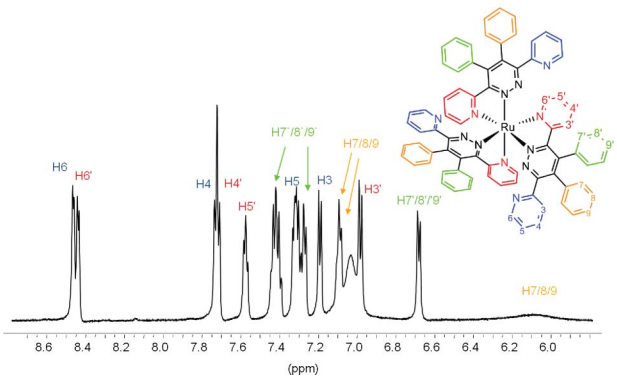

Fig. 4 The ^{1}H-NMR spectrum of *fac*-[Ru(**3a**)$_3$][PF$_6$]$_2$ (CD$_3$CN, RT, 600 MHz).

UV-Vis spectroscopy

The UV-Vis absorption spectra of both isomers of [Ru(**3a–5a**)$_3$]-[PF$_6$]$_2$ are shown in Fig. 5. The absorption maxima are bathochromically shifted (~λ 20 nm) relative to [Ru(bpy)$_3$]$^{2+}$ [29] due

Table 1 The oxidation and reduction potentials obtained for [Ru(**1a–6**)(bpy)$_2$][PF$_6$]$_2$ in CH$_3$CN (1 mM) with 0.1 M TBAPF$_6$ as supporting electrolyte. Recorded at RT using a glassy carbon working electrode, a Pt wire counter electrode and a SCE reference electrode

[Ru(L)(bpy)$_2$][PF$_6$]$_2$ L =	Oxidation *vs.* SCE/V	Reduction *vs.* SCE/V			$\Delta E_{\frac{1}{2}}$/V
1a	+1.48	–0.92	–1.39	–1.64	2.40
2a	+1.34	–0.98	–1.43	–1.64	2.32
3a	+1.39	–1.04	–1.42	–1.66	2.43
4a	+1.36	–0.91	–1.46	–1.67	2.27
5a	+1.43	–1.07	–1.42	–1.67	2.51
6	+1.28	–0.94	–1.46	–1.67	2.22

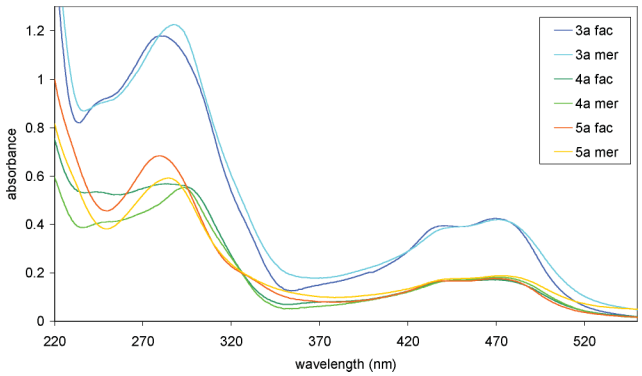

Fig. 5 The UV-Vis absorption spectra of the *fac* and *mer* isomers of $[Ru(\mathbf{3a–5a})_3][PF_6]_2$ (2×10^{-5} in CH_3CN).

to the increased electron withdrawing character of the pyridazine ring. The most interesting feature of the spectra is the small but consistent bathochromic shift of the *mer* isomers relative to their *fac* counterparts. This is as a result of the reduced symmetry associated with the *mer* isomer, and the loss of degeneracy in the ligands' π* orbitals.

The emission spectra of $[Ru(\mathbf{3a–5a})_3][PF_6]_2$ are shown in Fig. 6. These spectra reflect a pattern similar to that of the absorption spectra: there is a small consistent bathochromic shift in the emission maxima wavelength for each *mer* isomer relative to its *fac* counterpart. This difference is most apparent for the complex of ligand **3a**, where the maximum of the *mer* isomer is red-shifted 27 nm compared to the *fac* isomer. The *fac* isomer of the complex $[Ru(\mathbf{4a})_3][PF_6]_2$ has the lowest energy emission of the three *fac* isomers (λ 638 nm), probably due to the lower energy of the π* orbitals arising from the electron-withdrawing effect of the 4-pyridyl substituents.

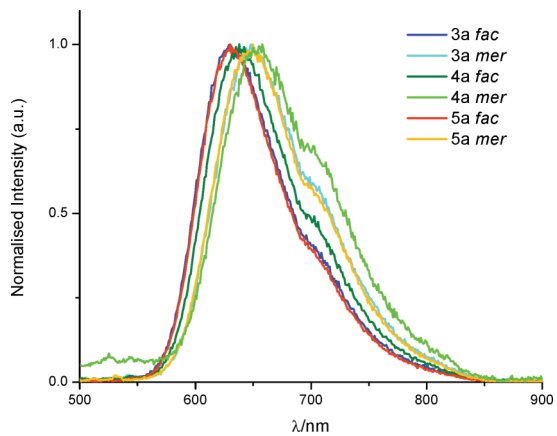

Fig. 6 The normalised emission spectra of the *fac* and *mer* isomers of $[Ru(L)_3][PF_6]_2$, for ligands **3a**, **4a** and **5a** in CH_3CN.

Iron(II) *tris*(homoleptic) complexes $[Fe(\mathbf{3a–5a})_3][PF_6]_2$

The meridional and facial isomers of the iron(II) complexes were similarly characterised by ^{1}H-NMR spectroscopy, mass spectrometry and UV-Vis spectroscopy. The ^{1}H-NMR spectra of the meridional isomers were complicated due to the lack of symmetry, however the methoxy protons were easily assigned, being the most shielded signals (ca. δ 3.6 ppm). The phenyl protons appear at δ 6.4 ppm, and the 2-pyridyl signals appear between δ 7.0 and 8.5 ppm. The *fac* isomer of $[Fe(\mathbf{5a})_3][PF_6]_2$ is drawn colour-coded along with its assigned ^{1}H NMR spectrum in Fig. 7. The proton signals were identified using a range of 2D-NMR techniques. Of particular note are the phenyl signals appearing between δ 6.0–7.0 ppm. The spectrum is similar to that of its ruthenium counterpart, with broadening observed in the signals associated with the aryl substituents. Assignments of the ^{1}H-NMR spectra of the *mer* and *fac* isomer of $[Fe(\mathbf{3a})_3][PF_6]_2$ and $[Fe(\mathbf{4a})_3][PF_6]_2$ were also obtained and are provided in the ESI.†

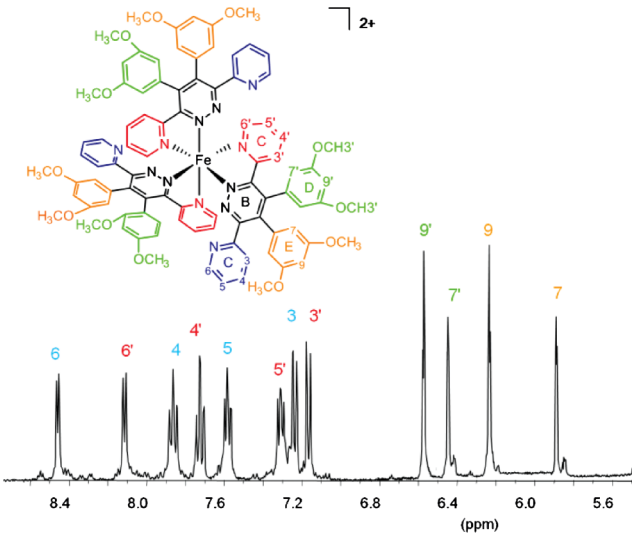

Fig. 7 The ^{1}H-NMR spectrum of the *fac* isomer of $[Fe(\mathbf{5a})_3][PF_6]_2$ (CD_3CN, RT, 600 MHz).

The UV-Vis absorption spectra of the *fac* and *mer* isomers of the three iron *tris*(homoleptic) complexes of ligands **3a**, **4a** and **5a** are shown in Fig. 8. The high-energy region of the spectra in each case is dominated by a ligand-centred π→π* transition which, for comparison appears at λ 298 nm in $[Fe(bpy)_3]^{2+}$.[30] Again, the meridional isomer of each complex absorbs at slightly longer wavelength than its facial analogue. The electron-withdrawing effects of the 4-pyridyl and the electron-donating effect of the methoxy substituents is evident in the slight shift in the absorption

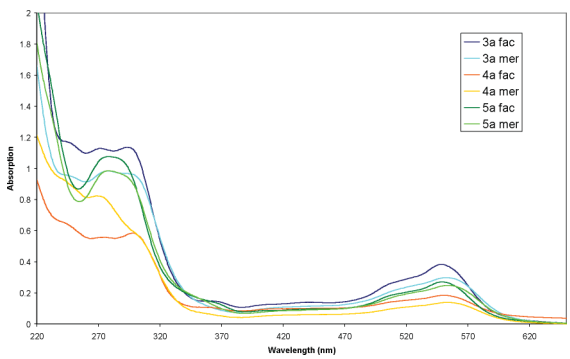

Fig. 8 The UV-Vis absorption spectra of the *fac* and *mer* isomers of $[Fe(\mathbf{3a–4a})_3][PF_6]_2$ (2×10^{-5} M in CH_3CN).

Table 2 Crystal data for complexes $[Ru(bpy)_2(\mathbf{1a})][PF_6]_2$, $[Ru(bpy)_2(\mathbf{2a})][PF_6]_2$, $[Ru(bpy)_2(\mathbf{6})][PF_6]_2$ and $[Ru(\mathbf{3a})_3][PF_6]_2$

Compound reference	$[Ru(bpy)_2(\mathbf{1a})][PF_6]_2\cdot(CH_3)_2CO$	$[Ru(bpy)_2(\mathbf{2a})][PF_6]_2\cdot(CH_3)_2CO$	$[Ru(bpy)_2(\mathbf{6})][PF_6]_2\cdot 3CH_2Cl_2$	$[Ru(\mathbf{3a})_3][PF_6]_2$
Chemical formula	$C_{42}H_{35}F_{12}N_9OP_2Ru$	$C_{41}H_{34}F_{12}N_{10}OP_2Ru$	$C_{47}H_{36}Cl_6F_{12}N_8P_2Ru$	$C_{78}H_{54}Cl_0F_{12}N_{12}O_0P_2Ru$
Formula mass	1072.80	1073.79	1316.55	1550.34
Crystal system	Monoclinic	Monoclinic	Monoclinic	Trigonal
a/Å	11.546(1)	10.986(1)	9.006(1)	18.443(4)
b/Å	19.751(2)	20.223(2)	43.982(3)	18.443(4)
c/Å	19.714(2)	20.344(2)	13.043(1)	12.820(3)
α/°	90.00	90.00	90.00	90.00
β/°	101.996(2)	104.637(2)	101.319(2)	90.00
γ/°	90.00	90.00	90.00	120.00
Unit cell volume/Å^3	4397.5(7)	4372.9(7)	5065.9(8)	3776(2)
T/K	173(2)	150(2)	150(2)	160(2)
Space group	$P2_1/c$	$P2_1/c$	$P2_1/c$	$P\bar{3}$
No. of formula units per unit cell, Z	4	4	4	2
No. of reflections measured	35681	35469	42101	9347
No. of independent reflections	8172	8141	9427	3936
R_{int}	0.0812	0.0447	0.1369	0.0561
Final R_1 values ($I > 2\sigma(I)$)	0.0526	0.0390	0.0804	0.0554
Final $wR(F^2)$ values ($I > 2\sigma(I)$)	0.1159	0.1009	0.1461	0.1251
Final R_1 values (all data)	0.0877	0.0548	0.1334	0.0942
Final $wR(F^2)$ values (all data)	0.1336	0.1119	0.1636	0.1362

maxima of the MLCT of complexes of **4a** and **5a** compared with the complexes of **3a**.

Crystallographic studies

The single crystal X-ray structures of the ligands **1a**, **2a**, **3a** and **6** are provided and discussed in the ESI.† The experimental and crystallographic data for the ruthenium complexes are detailed here and summarised in Table 2.

Crystals of $[Ru(\mathbf{2a})(bpy)_2][PF_6]_2$ were grown by slow evaporation of diethylether into an acetone solution of the complex. The complex crystallised in a monoclinic space group, $P2_1/c$. The asymmetric unit consists of the octahedral complex species along with two PF_6^- counter ions and an acetone molecule. The ligands are coordinated in an octahedral arrangement around the central metal as shown in Fig. 9. Rings C and D are tilted at angles of 33.45° and 48.61° respectively from the plane of the coordinated rings A and B. The Ru–N bond lengths vary between 2.014(2) Å and 2.068(2) Å. Four molecules of $[Ru(\mathbf{2a})(bpy)_2]^{2+}$ undergo self-assembly through the formation of C–H···N hydrogen bonds involving both the 2-pyridyl (H···N, 2.38 Å) and the pyrimidyl units (H···N, 2.56 Å). This leads to the formation of a host–guest framework, with two acetone molecules and two PF_6^- anions occupying the void space (Fig. 9). The guest species is held to the host-framework through C–H···O (H···O, 2.42, 2.45 Å) and C–H···F (with H···F distance varying from 2.31 to 2.53 Å) interactions. Unlike many such porous assemblies, the void space is not extended further to form a channel.

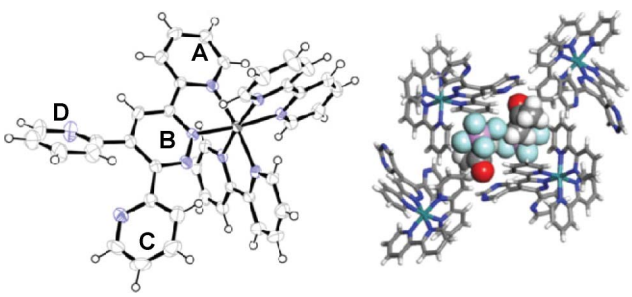

Fig. 9 Ortep representation of the crystal structure of $[Ru(\mathbf{2a})(bpy)_2][PF_6]_2$, (ellipsoids shown at 50% probability), the host–guest interaction observed is illustrated on the right.

Crystals of $[Ru(\mathbf{1a})(bpy)_2]^{2+}$ were grown by slow evaporation of diethylether into an acetone solution of the complex. This mixture yielded a complex, isostructural with that of $[Ru(\mathbf{2a})(bpy)_2]^{2+}$ (space group $P2_1/c$).

Crystals of $[Ru(\mathbf{6})(bpy)_2]^{2+}$ were obtained *via* recrystallisation from a dichloromethane/hexane mixture. The asymmetric unit consists of two PF_6^- counter ions and three dichloromethane molecules, crystallising in the monoclinic $P2_1/c$ space group. The Ru–N bond lengths are typical, ranging from 2.030(5) Å to 2.074(5) Å. The crystal packing is presented in Fig. 10.

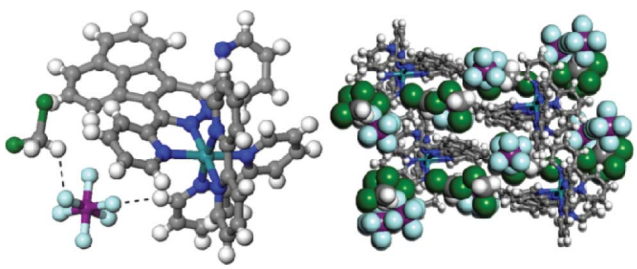

Fig. 10 Representations of the lattice structures of $[Ru(\mathbf{6})(bpy)_2][PF_6]_2$.

A crystal of *fac*-$[Ru(\mathbf{3a})_3][PF_6]_2$ suitable for single crystal X-ray diffraction was grown by slow diffusion of diethylether into an acetone solution of the complex (see Fig. 11). The complex crystallised in a $P\bar{3}$ trigonal space group and the unit cell contains two complex molecules and two $[PF_6]^-$ equivalents. The ruthenium(II) metal centre occupies a crystallographic special position at the 3-fold centre of symmetry and the anions are distributed across three sites (see Figure S3†). The host-framework comprises a layered arrangement of the metal centres with the

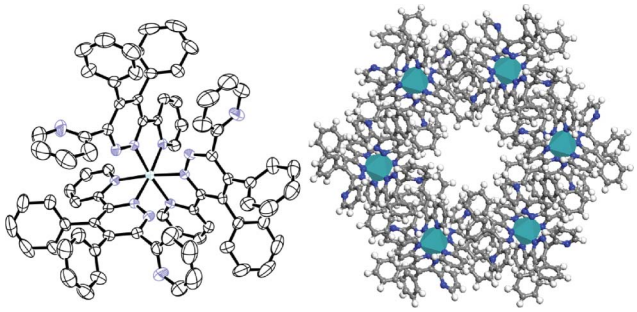

Fig. 11 *Left*: Ortep representation of the crystal structure of *fac*-[Ru(**3a**)(bpy)$_2$][PF$_6$]$_2$ (ellipsoids shown at 50% probability, counterions removed for clarity). *Right*: A representation of the hexagonal packing arrangement (Ru(II) centres shown as turquoise octahedra. (Counterions removed for clarity.)

anions lying in different planes. The bond lengths between the ruthenium metal and the pyridine and pyridazine nitrogen donor atoms are similar; 2.059(4) Å and 2.007(4) Å respectively. An ORTEP[31] representation of the complex cation is shown in Fig. 11, alongside a representation of the packing arrangement observed down the c axis. The complex forms a porous assembly which is stabilised by weak intermolecular $\pi\cdots\pi$ (3.481 Å) and C–H$\cdots$F (2.546 Å–2.650 Å) interactions

Conclusion

A family of substituted pyridazines, arising from inverse electron demand [2 + 4] Diels–Alder reactions between tetrazines and suitable dienophiles including acenaphthalene, have been structurally characterised and their crystal packing arrangements examined. The optical and electrochemical properties of these species as ligands in Fe(II) and Ru(II) *bis*(byridyl) and *tris*(homoleptic) complexes were shown to depend on the electron withdrawing nature of the pyridazine. The separation of both *mer* and *fac* isomers of the *tris*(homoleptic) complexes was serendipitously achieved *via* simple chromatographic separation on silica, avoiding the use of more complex separation strategies. This allowed for a spectral comparison of the properties of the geometric isomers. In each case the *mer*-isomers were found to exhibit a slight but consistent red-shift in the emission and absorption spectra. In one case the *fac*-isomer was structurally characterised revealing the potential of such symmetric complexes with multiple metal coordination modes in supramolecular frameworks. The work pushes forward the possibility of using preformed geometrically separable isomers as predirecting supramolecular motifs.[32]

Experimental section

Full experimental details are available in the ESI.† CCDC 812335–812342 contain the supplementary crystallographic data for this paper.†.

Acknowledgements

We wish to acknowledge the technical contribution of Drs John O'Brien, Manuel Ruether and Martin Feeney. We also wish to thank Dr Chris Fitchett for additional crystallographic support and Dr Han Vos (Dublin City University) for kindly providing the deuterated ligands. We acknowledge the funding provided by SFI- 05PICA819 (GC, SV) and IRCSET-PG07 (GMOM), LW EU-FP6 MKTD-011472 and SFI-PICA-1819 (RQ).

Notes and references

1 D. J. Gregg, E. Bothe, P. Höfer, P. Passaniti and S. M. Draper, *Inorg. Chem.*, 2005, **44**, 5654–5660.
2 D. J. Gregg, C. M. Fitchett and S. M. Draper, *Chem. Commun.*, 2006, 3090–3092.
3 D. J. Gregg, C. M. A. Ollagnier, C. M. Fitchett and S. M. Draper, *Chem. Eur. J.*, 2006, **12**, 3043–3052.
4 S. Varughese, G. Cooke and S. M. Draper, *CrystEngComm*, 2009, **11**, 1505–1508.
5 W. Kaim, *Coord. Chem. Rev.*, 2002, **230**, 127–139.
6 B. Gil, G. A. Cooke, D. Nolan, G. M. Ó Máille, S. Varughese, L. Wang and S. M. Draper, *Dalton Trans.*, 2011, DOI: 10.1039/c1dt10275c.
7 E. C. Constable, C. E. Housecroft, M. Neuburger, S. Reymann and S. Schaffner, *Chem. Commun.*, 2004, 1056–1057.
8 R. Hoogenboom, G. Kickelbick and U. S. Schubert, *Eur. J. Org. Chem.*, 2003, 4887–4896.
9 F. Thébault, A. J. Blake, C. Wilson, N. R. Champness and M. Schröder, *New J. Chem.*, 2006, **30**, 1498–1508.
10 A. M. M. Lanfredi, A. Tiripicchio and F. Ugozzoli, *J. Chem. Soc., Dalton Trans.*, 1988, 651–656.
11 N. Tsukada, T. Sato, H. Mori, S. Sugawara, C. Kabuto, S. Miyano and Y. Inoue, *J. Organomet. Chem.*, 2001, **627**, 121–126.
12 E. C. Constable, C. E. Housecroft, B. M. Kariuki, N. Kelly and C. B. Smith, *Inorg. Chem. Commun.*, 2002, **5**, 199–202.
13 M.-T. Youinou, N. Rahmouni, J. Fischer and J. A. Osborn, *Angew. Chem., Int. Ed. Engl.*, 1992, **31**, 733–735.
14 G. Baum, E. C. Constable, D. Fenske, C. E. Housecroft, T. Kulke, M. Neuburger and M. Zehnder, *J. Chem. Soc., Dalton Trans.*, 2000, 945–959.
15 C. M. Elliott and E. J. Hershenhart, *J. Am. Chem. Soc.*, 1982, **104**, 7519–7526.
16 H. Weizman, J. Libman and A. Shanzer, *J. Am. Chem. Soc.*, 1998, **120**, 2188–2189.
17 N. C. Fletcher, *J. Chem. Soc., Perkin Trans. 1*, 2002, 1831–1842.
18 A. V. Nemukhin, B. L. Grigorenko and A. A. Granovsky, *Moscow University Chemistry Bulletin.*, 2004, **45**, 75.
19 M. Kyakuno, S. Oishi and H. Ishida, *Inorg. Chem.*, 2006, **45**, 3756–3765.
20 S. Torelli, S. Delahaye, A. Hauser, G. Bernadinelli and C. Piguet, *Chem.–Eur. J.*, 2004, **10**, 3503–3516.
21 N. C. Fletcher, M. Nieuwenhuyzen and S. Rainey, *J. Chem. Soc., Dalton Trans.*, 2001, 2641–2648.
22 R. Ragni, E. A. Plummer, K. Brunner, J. W. Hofstraat, F. Babudri, G. M. Farinola, F. Naso and L. D. Cola, *J. Mater. Chem.*, 2006, **16**, 1161–1170.
23 G. Tresoldi, S. L. Schiavo and P. Piraino, *Inorg. Chim. Acta*, 1997, **254**, 381–385.
24 J. F. Geldard and F. Lions, *J. Org. Chem.*, 1965, **30**, 318–319.
25 B. Sarkar, W. Kaim, T. Schleid, I. Hartenbach and J. Fiedler, *Z. Anorg. Allg. Chem.*, 2003, **629**, 1353–1357.
26 S. Ernst and W. Kaim, *J. Am. Chem. Soc.*, 1986, **108**, 3578–3586.
27 S. Ernst and W. Kaim, *Inorg. Chim. Acta*, 1986, **114**, 123–125.
28 E. Ioachim, E. A. Medlycott, G. S. Hanan, F. Loiseau, V. Ricevuto and S. Campagna, *Inorg. Chem. Commun.*, 2005, **8**, 559–563.
29 A. Juris, V. Balzani, F. Barigalletti, S. Campagna, P. Belser and A. Von Zelewsky, *Coord. Chem. Rev.*, 1988, **84**, 85–277.
30 R. A. Kirgan and D. P. Rillemna, *J. Phys. Chem. A*, 2007, **111**, 13157–13162.
31 L. Farrugia, *J. Appl. Crystallogr.*, 1997, **30**, 565.
32 C. M. Ollagnier, D. Nolan, C. M. Fitchett and S. M. Draper, *Inorg. Chem. Commun.*, 2007, **10**, 1045–1048.

